TU Delft

Delft University of Technology

Linear and Non-Linear Dynamics of a Micro-ramp Wake

Groot, Koen; Casacuberta Puig, Jordi; Ye, Qingqing; Hickel, Stefan

Publication date
2019

Document Version
Final published version

Published in
ERCOFTAC bulletin

Citation (APA)
Groot, K., Casacuberta Puig, J., Ye, Q., & Hickel, S. (2019). Linear and Non-Linear Dynamics of a Micro-ramp Wake. *ERCOFTAC bulletin*, (118), 5-10.

Important note
To cite this publication, please use the final published version (if applicable).
Please check the document version above.

Copyright
Other than for strictly personal use, it is not permitted to download, forward or distribute the text or part of it, without the consent of the author(s) and/or copyright holder(s), unless the work is under an open content license such as Creative Commons.

Takedown policy
Please contact us and provide details if you believe this document breaches copyrights.
We will remove access to the work immediately and investigate your claim.

This work is downloaded from Delft University of Technology.
For technical reasons the number of authors shown on this cover page is limited to a maximum of 10.

European Research Community on Flow, Turbulence and Combustion

ERCOFTAC is a leading European association of research, education and industry groups in the technology of flow, turbulence and combustion. The main objectives of *ERCOFTAC* are: To promote joint efforts of European research institutes and industries with the aim of **exchanging technical and scientific information**; to promote **Pilot Centres** for collaboration, stimulation and application of research across Europe; to stimulate, through the creation of **Special Interest Groups**, wellcoordinated European-wide research efforts on specific topics; to stimulate the creation of advanced training activities; and to be influential on funding agencies, governments, the European Commission and the European Parliament.

www.ercoftac.org

Honorary President

Mathieu J.

Executive Committee

Chairman	Tomboulides, A. Aristotle University of Thessaloniki, Greece Tel: +30 2310 996068 ananiast@auth.gr
First Deputy Chairman	Von Terzi, D.
Treasurer	Hirsch, C.
SPC Chairman	Hickel, S.
SPC Deputy Chairman	Geurts, B.
KNC Chairman	Standingford, D.
KNC Deputy Chairman	Hillewaert, K.
Knowledge Base Editor	Rodi, W.
Bulletin Editor	Elsner, W.

ERCOFTAC Seat of the Organisation

Director	Hirsch, C. Chaussée de la Hulpe 189 Terhulpsesteenweg B-1170 Brussels, Belgium Tel: +32 2 643 3572 Fax:+32 2 647 9398 ado@ercoftac.be

Scientific Programme Committee

Chairman	Hickel, S. Delft University of Technology Faculty of Aerospace Engineering Kluyverweg 1 2629 HS Delft The Netherlands Tel: +31 152 789 570 S.Hickel@tudelft.nl
Deputy Chairman	Geurts, B.

Knowledge Network Committee

Chairman	Standingford, D. Zenotech Ltd. 1 Laarkfield Grove Chepstow,NP16 5UF United Kingdom Tel: +44 7870 628 916 david.standingford@zenotech.com
Deputy Chairman	Hillewaert, K

ERCOFTAC Central Administration and Development Office (CADO)

Admin. Manager	Jakubczak, M. PO Box 53877 London, SE27 7BR United Kingdom Tel: +44 203 602 8984 admin@cado-ercoftac.org Skype: Ercoftaccado

Table Of Contents

PREFACE: Laminar-Turbulent Transition Prediction and Control 4
A. Hanifi

Linear and Non-Linear Dynamics of a Micro-ramp Wake 5
K. J. Groot, J. Casacuberta, Q. Ye and S. Hickel

Recirculating Large Scale Structures Inside the Cove of a Bulb Sealed Slat 11
F. H. T. Himeno, D. S. Souza, D Rodriguez and M. A. F. Medeiros

Rossiter Modes in a Compressible Open Cavity: A Comparison Between the Linear Predictions and Non-linear Simulations 16
M. S. Mathias and M. A. F. Medeiros

Resolvent Analysis: With or Without Eddy Viscosity? 20
P. Morra, O. Semeraro, D. S. Henningson and C. Cossu

Uncertainty Quantification of Acoustic Receptivity with an Adjoint Linear Navier-Stokes Approach 25
H. Raposo, S. Mughal and R. Ashworth

On the Wave-cancelling Nature of Boundary Layer Transition Control 31
K. Sasaki, P. Morra, A. V. G. Cavalieri, A. Hanifi and D. S. Henningson

Editor Marek, M.

Technical Editor Kuban, Ł.

Chairman Elsner, W.

Editorial Board Armenio, V.
Dick, E.
Geurts, B.J.

Design & Layout Borhani, N.
Nichita, B.A.

Cover Design Aniszewski, W.

Submissions

ERCOFTAC Bulletin
Institute of Thermal Machinery
Częstochowa University of Technology
Al. Armii Krajowej 21
42-201 Częstochowa
Poland
Tel: +48 343 250 507
Fax: +48 343 250 507
Email:ercoftac@imc.pcz.czest.pl

Hosted, Printed & Distributed By

Częstochowa University of Technology

ISSN: 2518-0991

The reader should note that the Editorial Board cannot accept responsibility for the accuracy of statements made by any contributing authors

Next *ERCOFTAC* Events

ERCOFTAC Spring Festival
15th of April, 2019
Brussels, Belgium

ERCOFTAC Committee Meetings
16th of April, 2019
Brussels, Belgium

Linear and Non-Linear Dynamics of a Micro-ramp Wake

K. J. Groot, J. Casacuberta, Q. Ye and S. Hickel

Faculty of Aerospace Engineering, TU Delft, Kluyverweg 1, 2629HS, Delft, The Netherlands

Abstract

Micro-ramps are deployed to prevent boundary layer separation by creating a momentum excess close to the wall. Through Direct Numerical Simulations (DNS) of the base, instantaneous and mean flow, we identify that the perturbation dynamics in the wake of the micro-ramp play an essential role in creating the near-wall momentum excess. To identify the origin of the perturbations, we deploy BiGlobal stability analysis on the laminar base flow. We demonstrate that the amplification of the most unstable linear mode is closely related to the time-averaged amplitude of the unsteady perturbations. The flow structure corresponding to this mode has a varicose symmetry with respect to the symmetry plane and matches with the early development of the hairpin vortices in the instantaneous flow field. It is concluded that the varicose instability supported by the laminar base flow represents the mechanism that generates the hairpins.

1 Introduction

Micro-ramps are passive flow control devices that were originally introduced to prevent separation in Shock-Wave/Boundary-Layer Interactions (SWBLIs) [1]. In particular, the micro-ramp wake counteracts the tendency of the boundary layer to separate through the installment of high-speed streaks close to the wall.

The consensus ascribes the creation of the high-speed streaks to the predominant flow feature in the wake: a pair of counter-rotating streamwise vortices *downstream* the micro-ramp, see figure 8 of Babinsky *et al.* [2]. This explanation for the high-speed streak is questioned by Wang *et al.* [3], who proposed that, instead, the mechanism consists of an exchange of high- and low-momentum *along the chord* of the micro-ramp. They argued that the vortex pair is incapable of entraining high-speed fluid toward the wall farther downstream in the wake.

Care has to be taken when discussing the action of the streamwise vortices. Blinde *et al.* [4] showed that these (primary) vortices do not exist far enough downstream of the micro-ramp, they find unsteady hairpin vortices instead. Accordingly, Bo *et al.* [5] hypothesised that the high-speed streaks are firstly generated by the streamwise (primary) vortex pair, but thereafter the hairpins inherit this role.

We contribute to this discussion by assessing the incompressible flow dynamics around the micro-ramp with Direct Numerical Simulation (DNS) and BiGlobal stability analysis. A detailed experimental measurement dataset is available for the incompressible flow case, see Ye *et al.* [6, 7]. Next to computing the instantaneous flow through DNS, we compute the laminar base flow through the use of Selective Frequency Damping (SFD, [8]). The access to the laminar base flow allows for: (1) isolating the role of unsteady perturbations in the creation of the high-speed streaks and (2) determining its linear stability, representing the origin of the hairpin vortices.

This article is arranged as follows: in §2, the base and mean flow are discussed briefly, including the means with which they are obtained. In §3, the deployed linear stability method is justified and elaborated upon. After presenting the modes that undergo a significant amplification in §3.2, the most unstable mode is compared against the DNS and experimental measurement data in §3.3. The appearance of 'duckling beaks' is discussed in §3.4. The article is concluded in §4.

2 Base and mean flow

The micro-ramp geometry and the flow parameters are based on a transitional case considered by Ye *et al.* [7], who analysed the micro-ramp wake through the use of tomographic Particle Image Velocimetry (tomo-PIV) in the open-jet low-speed windtunnel (W-tunnel) of TU Delft. In particular, the case corresponding to the Reynolds numbers:

$$Re_h = \overline{U}_\infty h/\nu = 700$$
$$Re_{hh} = \overline{U}_h h/\nu = 468$$

is considerd here, where h represents the micro-ramp height, $\overline{U}_\infty$ is the freestream velocity, $\overline{U}_h$ the undisturbed streamwise velocity at the micro-ramp height and ν the freestream kinematic viscosity. The interrogation volume used was $0.57h \times 0.29h \times 0.57h$ in xyz-space and a 75% overlap was deployed; the resulting resolution allowed for obtaining high-quality spatial flow derivative fields. For further details see Ye *et al.* [6, 7].

The DNS is performed with INCA [9, 10]. A third order explicit Runge-Kutta method is used to march the solution in time, a 5th-order Weighted Essentially Non-Oscillatory (WENO) scheme is used to discretize space on a high-resolution structured grid. This grid ensures $y^+ < 1$ around the micro-ramp and near the wall and a high resolution of the shear layer in the wall-normal direction. Next to the simulation of the instantaneous flow over a long enough time period to ensure a converged mean flow, Selective Frequency Damping (SFD) is deployed to obtain the unstable base flow. Details of the DNS and SFD technique are reported independently in [11].

2.1 Flow overview

Streaks are here defined as isosurfaces of $\overline{U}_{\text{str}} = \overline{U} - \overline{U}_{\text{un}}$, where $\overline{U}_{\text{un}}$ is the streamwise velocity of the undisturbed boundary layer flow. The streaks in the base and mean flow are displayed in Figure 1; red and blue surfaces respectively indicate velocity-deficit and -excess streaks. Subfigures (b) and (c) show the good match between the mean flows obtained through DNS and tomo-PIV,

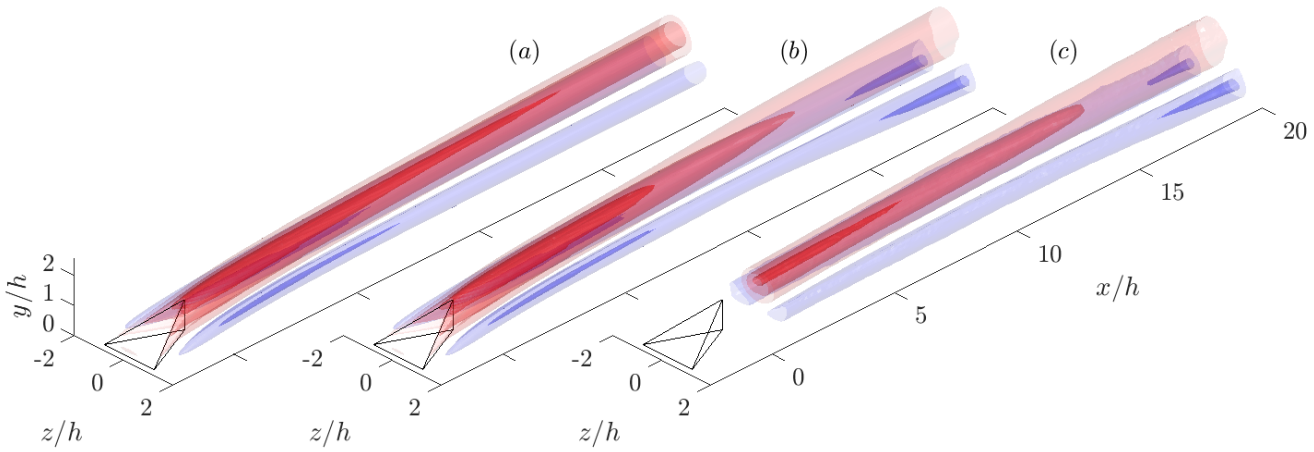

Figure 1: Streamwise velocity streaks ($\overline{U}_{\rm str}/\overline{U}_\infty = +0.2$ and $+0.1$ (blue) and -0.1, -0.3 and -0.5 (red)) in the (a) computed base, (b) computed mean and (c) measured mean (tomo-PIV by Ye *et al.* [7]) flow behind the micro-ramp

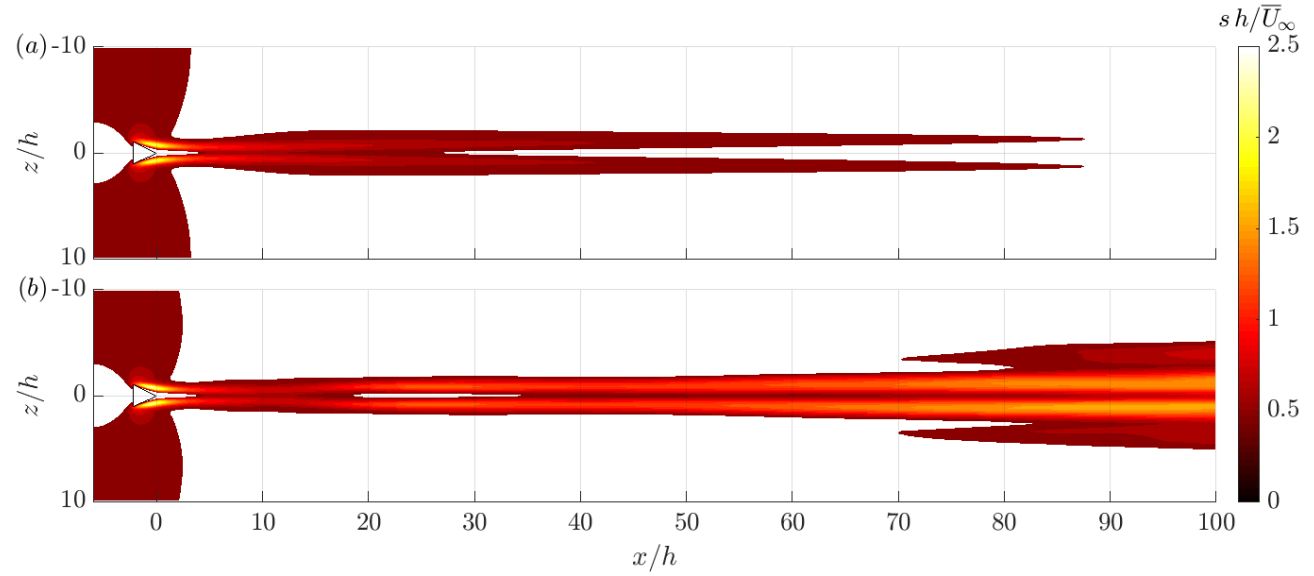

Figure 2: Strain rate magnitude, s, at the wall in the computed (a) base and (b) mean flow

while subfigures (a) and (b) represent a comparison of the computed base and mean flow. The most important difference between the base and mean flow is that the isosurface $\overline{U}_{\rm str}/\overline{U}_\infty = +0.2$ reappears in the mean flow for $x/h > 17$, while it does not in the base flow. This observed behaviour of the velocity-excess streak persists further downstream in the domain.

The strain rate of the flow at the wall is an important factor in relation to the prevention of boundary layer separation. Figure 2 shows its magnitude in the computed base (a) and mean (b) flow solutions. Marked differences are observed, which are attributed the action of perturbations on the mean flow. The vortices in the base flow are found to be incapable of maintaining the entrainment of momentum into the boundary layer and, consequently, are also incapable of maintaining the strain rate at the wall. A more detailed analysis of the differences between the base and mean flow is presented independently, see Casacuberta *et al.* [11].

Unsteady perturbations clearly play an important role in maintaining and enhancing the high-speed streaks. For this reason, the perturbations' existential origin is investigated next through analysing the stability of the base flow to infinitesimal perturbations.

3 Stability analysis

Infinitesimal perturbations to flows are governed by the linearized Navier-Stokes equations in general. Specific features of the base flow under investigation allow imposing further simplifications that reduce the complexity of the analysis. In particular, the separated-/reverse-flow region behind the micro-ramp is very small; it is limited to $x/h < 1$, see Figure 3. This is argued to be the result of the slender shape of the micro-ramp and the action of the streamwise vortices. For $x > h$, the flow develops slowly in the streamwise direction, which justifies the use of the spanwise BiGlobal stability framework [12], in which the impact of streamwise gradients of the base flow on perturbations is neglected.

3.1 BiGlobal stability method

This assumption can be made explicit with the perturbation ansatz associated to the spanwise BiGlobal (also referred to as the BiLocal) stability framework as follows:

$$q(x,y,z,t) = \overline{Q}(y,z) + \tilde{q}(y,z)\,\mathrm{e}^{\mathrm{i}(\alpha x - \omega t)} + c.c., \qquad (1)$$

where q denotes an instantaneous flow quantity, $\overline{Q}$ represents a base flow quantity, $\tilde{q}$ is a (complex) perturbation amplitude, ω the angular frequency, α the streamwise

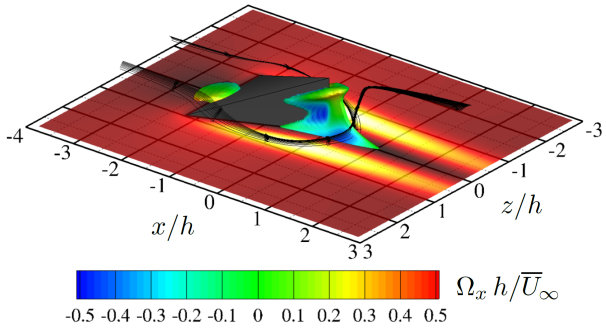

Figure 3: Reverse flow regions (indicated by $\overline{U} = 0$ isosurfaces) colour-coded by streamwise vorticity, Ω_x

wavenumber and *c.c.* denotes '*c*omplex *c*onjugate.' This ansatz is used specifically for the velocity components in the streamwise x-, wall-normal y- and spanwise z-direction: u, v and w, respectively, and the pressure p. Here, perturbation quantities are defined as: $q' = q - \overline{Q}$.

Substituting this ansatz into the linearized Navier-Stokes equations yields the spanwise BiGlobal stability equations:

$$-\mathrm{i}\omega\,\tilde{u} + \mathrm{i}\alpha\,\overline{U}\,\tilde{u} + \overline{V}\,\frac{\partial\tilde{u}}{\partial y} + \overline{W}\,\frac{\partial\tilde{u}}{\partial z} + \tilde{v}\,\frac{\partial\overline{U}}{\partial y} + \tilde{w}\,\frac{\partial\overline{U}}{\partial z} = -\mathrm{i}\alpha\,\tilde{p} + \frac{1}{Re}\left(-\alpha^2 + \frac{\partial^2}{\partial y^2} + \frac{\partial^2}{\partial z^2}\right)\tilde{u}; \tag{2a}$$

$$-\mathrm{i}\omega\,\tilde{v} + \mathrm{i}\alpha\,\overline{U}\,\tilde{v} + \overline{V}\,\frac{\partial\tilde{v}}{\partial y} + \overline{W}\,\frac{\partial\tilde{v}}{\partial z} + \tilde{v}\,\frac{\partial\overline{V}}{\partial y} + \tilde{w}\,\frac{\partial\overline{V}}{\partial z} = -\frac{\partial\tilde{p}}{\partial y} + \frac{1}{Re}\left(-\alpha^2 + \frac{\partial^2}{\partial y^2} + \frac{\partial^2}{\partial z^2}\right)\tilde{v}; \tag{2b}$$

$$-\mathrm{i}\omega\,\tilde{w} + \mathrm{i}\alpha\,\overline{U}\,\tilde{w} + \overline{V}\,\frac{\partial\tilde{w}}{\partial y} + \overline{W}\,\frac{\partial\tilde{w}}{\partial z} + \tilde{v}\,\frac{\partial\overline{W}}{\partial y} + \tilde{w}\,\frac{\partial\overline{W}}{\partial z} = -\frac{\partial\tilde{p}}{\partial z} + \frac{1}{Re}\left(-\alpha^2 + \frac{\partial^2}{\partial y^2} + \frac{\partial^2}{\partial z^2}\right)\tilde{w}; \tag{2c}$$

$$\mathrm{i}\alpha\,\tilde{u} + \frac{\partial\tilde{v}}{\partial y} + \frac{\partial\tilde{w}}{\partial z} = 0. \tag{2d}$$

Perturbation amplitudes $\{\tilde{u}, \tilde{v}, \tilde{w}, \tilde{p}\}$ are sought that are dominant in the shear layers in the wake and decay far away from these layers. This property justifies truncating the zy-plane. Specifically, the domain is chosen such that: $(z, y)/h \in [-5.5, 5.5] \times [0, 13.4]$. Truncation boundary conditions must be imposed to close the system. At the wall, $y = 0$, the no-slip condition is imposed for all velocity amplitudes and the y-momentum equation is used as a compatibility condition for the pressure amplitude. Dirichlet conditions are used for the velocity amplitudes at all truncation boundaries. Neumann conditions are imposed on the pressure at the boundaries in the spanwise direction, while a Dirichlet condition is imposed at the top boundary, for this resolves the additive non-uniqueness of the pressure field. The results are independent of the domain lengths and the chosen boundary conditions.

We are interested in perturbations that grow in the streamwise direction. Therefore a (real) frequency is imposed, implying zero temporal amplification. Given the boundary conditions, the base flow evaluated at a zy-plane at a downstream x-station of the micro-ramp and the frequency ω, 2 forms a quadratic eigenvalue problem, where α is the eigenvalue and $\tilde{u}$, $\tilde{v}$, $\tilde{w}$ and $\tilde{p}$ are eigenfunctions. The quadratic problem is cast into a linear eigenvalue problem through the companion matrix approach [13].

The problem is discretized using Chebyshev collocation [14] in both the z- and y-direction. A BiQuadratic mapping is used [15], that places one-third of the collocation nodes in-between specified coordinate locations, e.g. y_{i1} and y_{i2} in the y-direction, so that a particular region in the interior of the domain can be resolved. This is required because the shear layers of interest are disjoint from the domain's boundaries. In particular, the parameters are chosen as follows:

$$(z_{i1}, z_{i2})/h = (-1.0, 1.0)$$
$$(y_{i1}, y_{i2})/h = \begin{cases} (1.0, 1.5) & \text{for: } x/h < 15 \\ (2.5, 3.5) & \text{for: } x/h \geq 15 \end{cases}$$

The mapping coordinates (y_{i1}, y_{i2}) are displaced to a higher location for $x/h \geq 15$. This is done to account for the movement of the shear layers with respect to the wall. Interpolation in the x-direction is avoided when plotting isosurfaces that involve the perturbation flow field, therefore the jump in the (y_{i1}, y_{i2})-values corresponds to a small interruption of the surfaces at $x/h = 15$. By using the combination of the mappings and the spectral order of the scheme, the use of 60 nodes in both z- and y-directions yielded α-eigenvalues converged up to $O(10^{-5})$ absolute errors in units of rad/h.

The base flow and its spatial derivatives must be known on the mapped collocation grid, which is distinct from the finite volume DNS grid. To this end, the quantities and their spatial derivatives, all consistent with the discretization of the base flow, are interpolated with a cubic spline.

The Arnoldi method is used to solve the problem [16]. A special guess for the α-eigenvalue is used:

$$\alpha\,h = 1.24\left(\frac{\omega\,h}{\overline{U}_\infty}\right)^{1.035}\left(1 + \frac{1.5}{\frac{x}{2h}+1}\right) + \mathrm{i}\left(0.05 - \frac{2}{\frac{x}{2h}+1}\right), \tag{3}$$

which is based on manually fitting a curve to the locus traced by the α-values corresponding to the most unstable modes through the α-plane when following them over the range $x/h \in [0, 60]$. Its use allowed minimising the number of requested modes per solve to 5 and this reduced the time required to solve an individual eigenvalue problem to approximately 7 minutes.

3.2 Significantly amplified modes

The negative of the imaginary part of the streamwise wavenumber, $-\alpha_i$, represents the spatial exponential growth rate of perturbations in the streamwise direction per considered x-station. By integrating this growth rate in x, one obtains the N-factor:

$$N(x) = -\int_{x_0}^{x} \alpha_i(\bar{x})\,\mathrm{d}\bar{x}, \tag{4}$$

where $\bar{x}$ represents the dummy-equivalent of the x-coordinate and x_0 usually indicates the x-coordinate corresponding to zero growth, i.e. $\alpha_i = 0$. Here, no such location could be found downstream of the micro-ramp, therefore x_0 is set to zero to yield consistent results.

The BiGlobal problem was solved for $x/h \in [0, 60]$ and $\omega\,h/\overline{U}_\infty = O(1)$. Two modes are found that attain significant N-factors in the considered x-range. Figure 4 shows the u'-isosurfaces corresponding to the eigenfunctions and Figure 5 the N-factor curves at the frequencies for which the largest N-factors are attained in the range $x/h \in [5, 10]$. The DNS displays significant perturbation amplification in this particular range. By inspection of

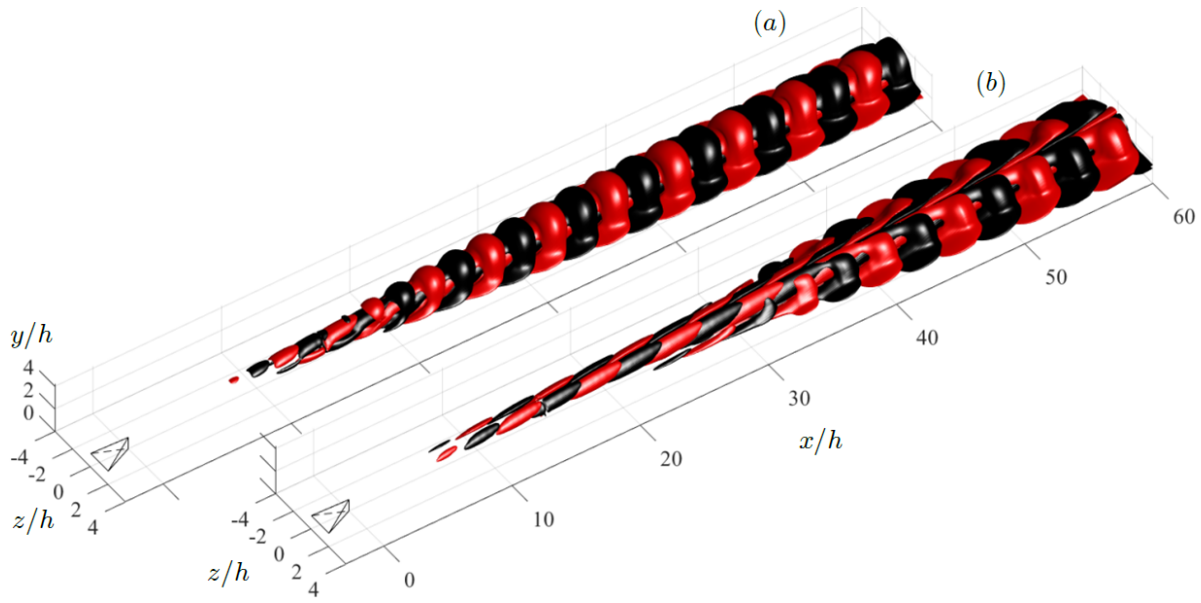

Figure 4: Isosurfaces of u' (red: positive, black: negative) for the most unstable (a) varicose and (b) sinuous modes

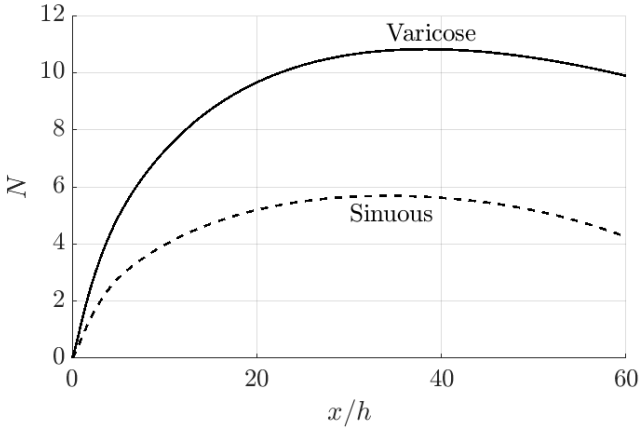

Figure 5: N-factors for most unstable frequencies of the varicose (solid line, $\omega\, h/\overline{U}_\infty = 1.4 \pm 0.1$) and sinuous (dashed, 1.3 ± 0.1) modes

the eigenfunctions, the modes are symmetric and anti-symmetric with respect to the center-plane, i.e. at $z = 0$; modes with these symmetries are also referred to as varicose and sinuous modes, respectively. The varicose instability mode is found to have an N-factor that is about twice as large as that corresponding to the sinuous mode. The varicose mode is therefore expected to dominate the perturbation dynamics at small amplitudes.

To construct the u'-isosurfaces shown in Figure 4, the $\tilde{u}$-eigenfunctions are stitched together at the considered x-stations (with a spacing of $0.25h$) to form the three-dimensional representation. Several steps were taken to do this. First, the phase of the eigenfunctions was aligned in the x-direction. This was done by letting the real part of the pressure amplitude function attain its absolute maximum, i.e. $\max_{z,y} \tilde{p}_r = \max_{z,y} |\tilde{p}|$, where the subscript r denotes the real part. The pressure eigenfunction was chosen, because it has a very well-defined (approximately spherical) shape. Second, the maximum amplitude of the $|\tilde{u}|$-eigenfunction, which have the largest overall amplitudes, were unified in the x-direction. The last two steps are allowed because a complex multiple of an eigenvector is again an eigenvector, where an eigenvector is the vector of eigenfunctions, like: $\Xi = [\tilde{u}, \tilde{v}, \tilde{w}, \tilde{p}]^T$. Third, the (varying) streamwise wavenumber and the relative amplitude dictated by the N-factor were imposed by multiplying the eigenfunctions with $\mathrm{e}^{N(x)+\mathrm{i}\alpha_r x}$ and, fourth, the real part was taken.

3.3 Comparison with DNS and experimental measurement data

Given that the varicose mode is expected to govern the perturbation dynamics at small amplitudes, the DNS data is probed for amplitude information and the spatial structure of perturbations. The amplitude information is extracted by integrating the mean normal Reynolds stress $\langle u'u' \rangle$ over zy-planes at every x-station yielding:

$$\epsilon^2_{rms} = \iint \frac{\langle u'u' \rangle}{\overline{U}^2_\infty} \frac{\mathrm{d}y\, \mathrm{d}z}{h^2}. \qquad (5)$$

Note that, due to the square appearance of u' in 5, this quantity is best compared against $\mathrm{e}^{2N(x)}$. Figure 6 shows that this comparison is highly successful. Figure 7 presents a comparison of the streamwise perturbation velocity isosurfaces. The match of the topology of the perturbation is striking; structures that are alike are labelled. The part labelled '3' evolves into a large arc that connects to the leg-like parts labelled '4'. This large arc surrounds the (not shown) negative counterpart of the part labelled '1', forming the head of the hairpin vortex. The part labelled '2' also evolves into a downward arch that connects to the leg-parts '4'. Despite the match of the topologies, the wavelength of the perturbation in the DNS is clearly smaller than that of the most unstable varicose mode. Identifying the cause of this difference requires a deeper investigation.

Performing POD reconstruction of the tomo-PIV experiment allowed Ye *et al.* [7] to represent the structure of the instantaneous flow field in terms of streamwise vorticity isosurfaces. Structures, referred to as 'leg-buffers', were identified that propagate away from the center-plane and may represent the onset of the spanwise propagation of the elevated strain-rate levels at the wall in the mean flow, see Figure 2. In Figure 8, the comparison is made against the instantaneous DNS data, in subfigure (b), and the base flow plus the eigenfunction corresponding to the most unstable varicose mode, in subfigure (a). The amplitude of the eigenfunction was set according to that shown in Figure 6. A match is found in regard to the topology of the surfaces in the instantaneous DNS

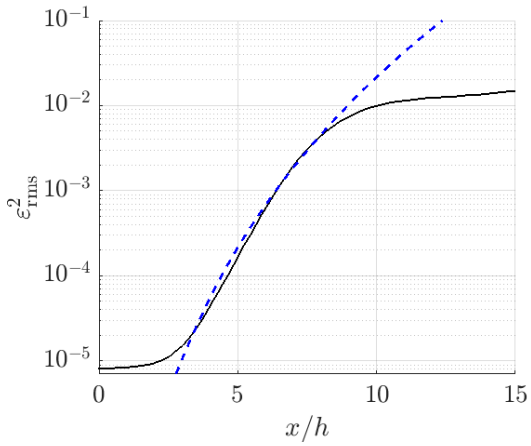

Figure 6: Comparison of the energy in the streamwise perturbation velocity component from DNS (solid line) and the $2N$-factor of the most unstable varicose mode (dashed)

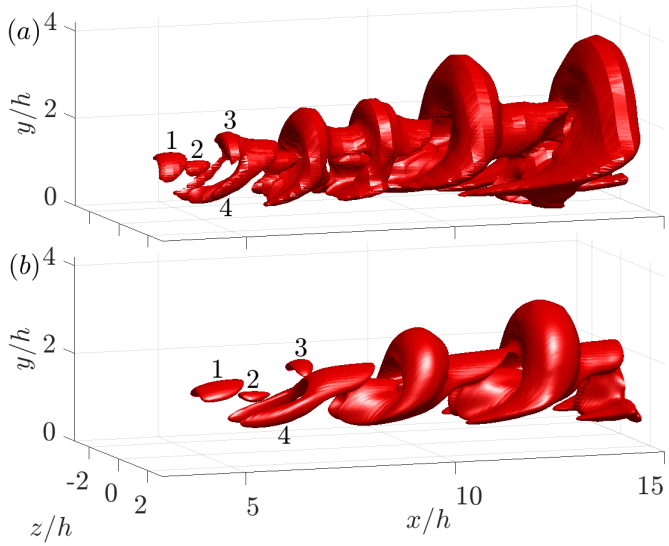

Figure 7: Isosurfaces of u' corresponding to (a) an instantaneous snapshot from DNS and (b) the varicose eigenmode. Matching perturbation structures are labelled

and measurement data. The fact that a match is established between computed and measured flows on the level of spatial derivatives of the flow deserves an emphasis. The larger wavelength in the measurement data, just like for the most unstable eigenmode, presents the most significant difference.

It is striking that, despite non-linear dynamics set in at approximately $x/h = 8$, the varicose eigenmode still represents some of the pertinent features of the dynamics for $x/h > 8$. In particular, the eigenmode seems to consist of a structure that propagates in the spanwise direction as its amplitude increases, similarly as the leg-buffers. This hints that insight into the origin of the leg-buffers can possibly be obtained by analysing the varicose eigenmode in further detail.

3.4 Duckling beaks

In a previous study of the stability of the micro-ramp wake, Groot *et al.* [17] presented Q-criterion isosurfaces of the base flow plus the varicose mode eigenfunction. Due to the quadratic nature of the Q-criterion, the resulting structure depended on the chosen finite amplitude of the eigenfunction. For a large enough amplitude a so-called 'duckling beak' appeared underneath the hairpin heads. Although this structure was labelled as an artifact, a very similar structure is observed in λ_2-isosurfaces of the presently analysed instantaneous DNS flow field, see Figure 9. Besides showing that this structure is physical, it moreover suggests the superharmonic (twice the streamwise wavenumber) of the varicose mode plays a role in the non-linear perturbation dynamics.

4 Conclusions

High-speed streaks found close to the wall in the wake of micro-ramps counteract the tendency of boundary layers to separate. It is demonstrated in this article that, at flow freestream speeds, the perturbation dynamics are essential in the prolongation of the high-speed streak far downstream of the micro-ramp. The origin of these perturbations is investigated with linear stability analysis.

Two significantly amplified instability modes are found; one has a varicose symmetry with respect to the center-plane, while the other has a sinuous symmetry. The varicose mode is most unstable and is therefore expected to dominate the perturbation dyanmics in the limit of infinitesimal amplitudes. When comparing the mode against the hairpin vortices found in the Direct Numerical Simulation (DNS) and tomo-graphic Particle Image Velocimetry (tomo-PIV) data, the amplitude evolution is matched and a topological match is established at small streamwise distances from the micro-ramp, where the perturbation amplitudes are significantly small. It can therefore be concluded that the varicose instability supported by the laminar base flow represents the mechanism that generates the hairpins. The most significant difference between the datasets is that the instantaneous DNS data features a perturbation with a smaller wavelength than the eigenmode and that observed in the measured flow field.

Surprisingly, the varicose mode seems to represent a spanwise propagation of the perturbations similar to the leg-buffers that Ye *et al.* [7] observe in the streamwise range for which non-linear dynamics have set in. This suggests that the origin of the leg-buffers can be investigated by performing a deeper analysis of the varicose eigenmode. Duckling beaks, earlier labelled as an artefact by Groot *et al.* [17], are recovered in the DNS. This demonstrates that they are, in fact, physical structures.

References

[1] B. H. Anderson, J. Tinapple, and L. Surber, "Optimal control of shock wave turbulent boundary layer interactions using micro-array actuation," *AIAA paper*, no. 3197, pp. 1–14, 2006.

[2] H. Babinsky, Y. Li, and C. W. Pitt Ford, "Microramp control of supersonic oblique shock-wave/boundary-layer interactions," *AIAA Journal*, vol. 47, no. 3, pp. 668–675, 2009.

[3] X. Wang, Y. Yan, Z. Sun, and C. Liu, "LES investigation into the generation of momentum deficits in the supersonic wake of a micro-ramp," *Journal of Mechanical Science and Technology*, vol. 28, no. 4, pp. 1327–1337, 2014.

[4] P. L. Blinde, R. A. Humble, B. W. Van Oudheusden, and F. Scarano, "Effects of micro-ramps on a shock wave/turbulent boundary layer interaction," *Shock Waves*, vol. 19, no. 6, p. 507, 2009.